NUMI note 2364
Version 1.0
October 31, 2006

Monte Carlo Studies of Rock Muons

A. McGowan, G. Giurgiu, M. Goodman

Argonne National Laboratory

Abstract

In this note we study the fitting procedure to be used in the measurement of the oscillation parameters $sin^2 2\theta$ and Δm^2_{32} using rock muons in the MINOS far detector. The rock muons are produced by beam neutrino interactions in the rock surrounding the far detector. We show that the fitting procedure is unbiased and the distribution of the fit outcomes on statistically independent Monte Carlo samples is consistent with the expected confidence contours. We find that significant sensitivity improvement can be achieved when including in the analysis the contained vertex events rejected by the main charge-current analysis.

1 Introduction

The sensitivity of rock muons to the oscillation parameters is lower than the sensitivity of contained events. However, the sensitivity of a rock muon analysis would be appreciable by the end of the MINOS running and will provide an independent measurement of the oscillation parameters. This independent measurement will provide a consistency check with the contained vertex analysis and it would result in a slight improvement of the overall measurement.

In this note we present Monte Carlo studies of neutrino induced rock muons in the MINOS far detector. In general, we distinguish between events with a true interaction vertex in the rock and those with a vertex in the detector. We start by performing a simple sensitivity study of rock vertex events using the counting rate only. Then, we study the event variables sensitive to neutrino oscillations: the reconstructed track momentum and direction with respect to the beam axis. Finally, we test the fitting procedure by comparing the input oscillation parameters with the fit outcomes, and analyze the distribution of fit outcomes on statistically independent samples.

2 Monte Carlo Sample

The Monte Carlo sample used for the studies presented in this note was generated using the standard GMINOS executable gminos_batch_carrot_08 and reconstructed using R1.18.2 minossoft. This includes all charged current and neutral current interactions arising from the standard v18 beam flux simulation (with ν_μ, $\overline{\nu_\mu}$ and ν_e components). Oscillations are not present in the simulation, but are added later in our study. Backgrounds are not present in this first sample. The sample corresponds to an exposure of 554.67×10^{20} protons on target (POT).

Event selection criteria are applied as follows. We require at least one reconstructed track. We require that the direction of the track is along the beam direction, $\cos\theta_{beam} > 0.5$ ($\theta_{beam} < 60°$), where θ_{beam} is the angle between the reconstructed track vertex and the beam direction. The track must originate from outside the detector, which means that the track vertex should be inside the detector, but close to the faces or outer surface of the detector. If the track enters the detector through the South (upstream) face, the vertex of the track must be within the first two planes of the detector. If the track enters through the lateral surfaces, the perpendicular distance between the track vertex and the outer surface must be less than 10 cm. Each track must have a valid measured momentum. For tracks that exit the detector, the momentum is measured by curvature. A track is considered as exiting the detector if the track end is contained within the last two planes of the detector or if the distance between the track end and the lateral surface of the detector is less than 10 cm. For momentum by curvature, tracks are selected if $q/p \neq 0$ and $|(q/p)/\sigma(q/p)| > 3.0$. All tracks that do not exit the detector are considered as stopped and the momentum is measured by range.

Table 1 shows a summary of the cuts and the number of events left after each cut. It is noted that we lose roughly 6% of all track events due to poor reconstruction of the curvature. These events may be recovered at a later time and combined into a rate-only bin for events

with ambiguous momentum.

Requirement	Events	Fraction (%)
no cuts	138243	-
at least one track	109272	100.0
cos $\theta_{beam} > 0.5$	108591	99.4
track originates from outside	104716	95.8
valid momentum measurement	97872	89.6
momentum from range	79267	72.5
momentum from curvature	18605	17.1

Table 1: Summary of event selection criteria and the events remaining after each cut.

To determine the distributions of different quantities in the presence of neutrino oscillations, we adopt the following procedure. We set the mixing angle and the mass difference to $sin^2 2\theta = 0.95$ and $\Delta m^2_{32} = 3.0 \times 10^{-3}\ eV^2$. For each event in the MC sample, given the true neutrino energy we determine the survival probability given by:

$$P(L, E; \theta, \Delta m_{32}) = 1 - sin^2 2\theta \times sin^2(1.27 \times \frac{\Delta m^2_{32} \times L(km)}{E(GeV)}). \quad (1)$$

When filling the oscillated histograms, each event is weighted by the survival probability given in the above equation.

Figure 1 shows in the top-left plot the true energy distributions of neutrinos in absence of oscillations with dotted line and in presence of oscillations with solid line. The ratio between the oscillated and un-oscillated true neutrino energy distributions is shown in the bottom-left plot. Similar distributions are shown in the same figure for the reconstructed muon track energy (middle) and angle with the beam axis (right). For rock events, the neutrino energy cannot be reconstructed since the neutrino interaction vertex is in the rock outside the detector. However, the reconstructed energy and angle of the track are correlated with the initial neutrino energy and can be used for measurement of the neutrino oscillation parameters $sin^2 2\theta$ and Δm_{32}. The ratios between the oscillated and un-oscillated distributions of the rock muon energy and angle are less than one for energies below 5 GeV and for all angles as seen in Figure 1. This is evidence that both energy and angle with the beam axis are sensitive to neutrino oscillations.

We study the correlations between the track energy and angle and find that the two quantities are not independent, as seen in Figure 2. For low energies, the angle between the rock muon direction and the beam axis tends to populate the whole range between $0.5 <$ cos $(\theta_{beam}) < 1.0$, while for high energies, the muons tend to be confined at small angles with the beam axis. However, the number of rock muons produced close to the beam axis is much larger than the number of muons that make a large angles.

Since the track energy and angle are correlated, we study the track energy distribution in three angle bins: $0.5 <$ cos $(\theta_{beam}) < 0.9$, $0.9 <$ cos $(\theta_{beam}) < 0.99$ and $0.99 <$ cos $(\theta_{beam}) < 1.0$. The corresponding oscillated and un-oscillated energy distributions are shown in Figure 3 as well as the ratios between oscillated and un-oscillated distributions. The ratios between oscillated and un-oscillated distributions show that muons with large angle with the

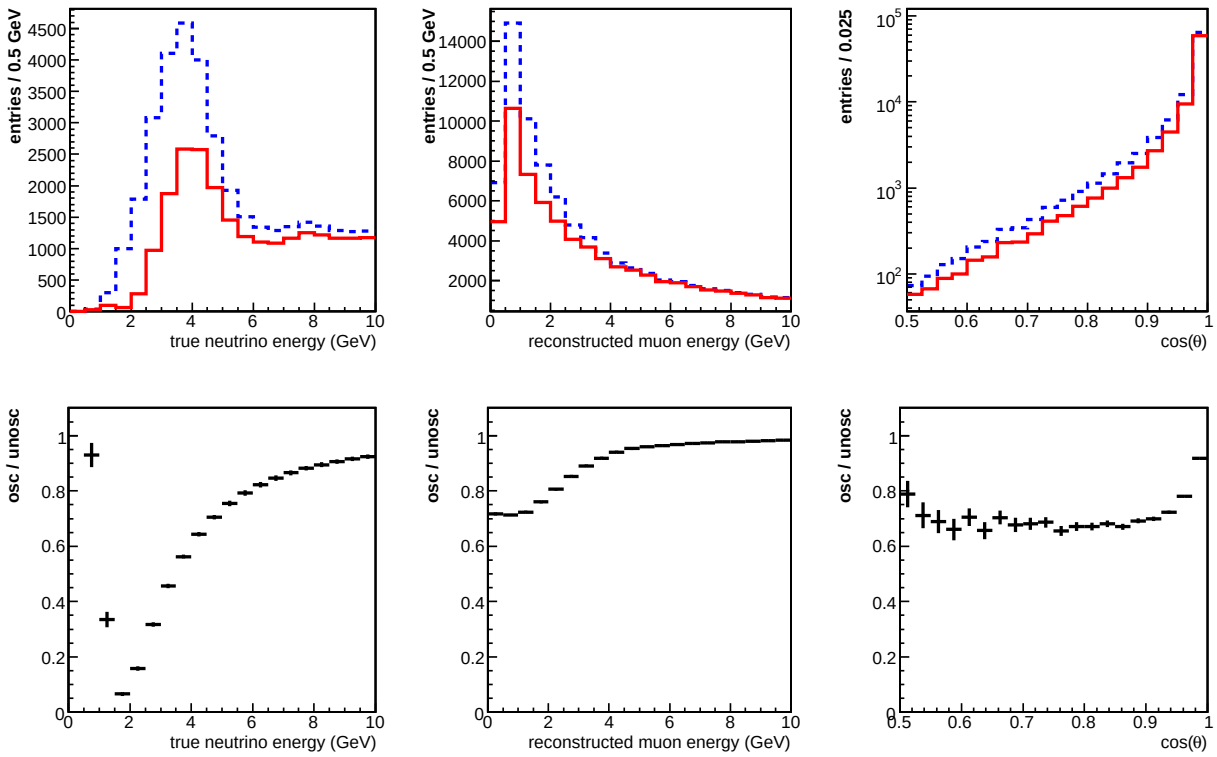

Figure 1: True energy of neutrinos (left), reconstructed track energy (middle), reconstructed track angle with beam axis (right). Dotted line corresponds to un-oscillated distributions, solid line corresponds to distributions of survived events in presence of oscillations. Points with error bars correspond to the ratio between oscillated and un-oscillated distributions.

beam axis are more sensitive to neutrino oscillations than muons that are confined close to the beam axis. We will take advantage of the dependence of sensitivity to oscillations to the angle θ_{beam} by separating the data in different θ_{beam} bins.

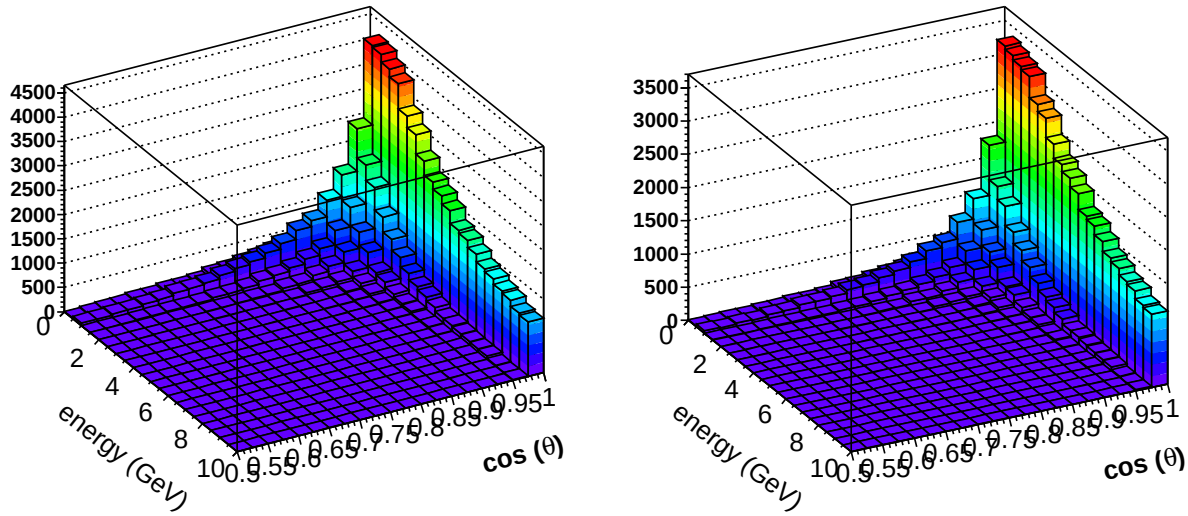

Figure 2: Correlation between the muon track energy and the angle of the muon with the beam direction cos θ_{beam}. Both un-oscillated (left) and oscillated (right) distributions are shown.

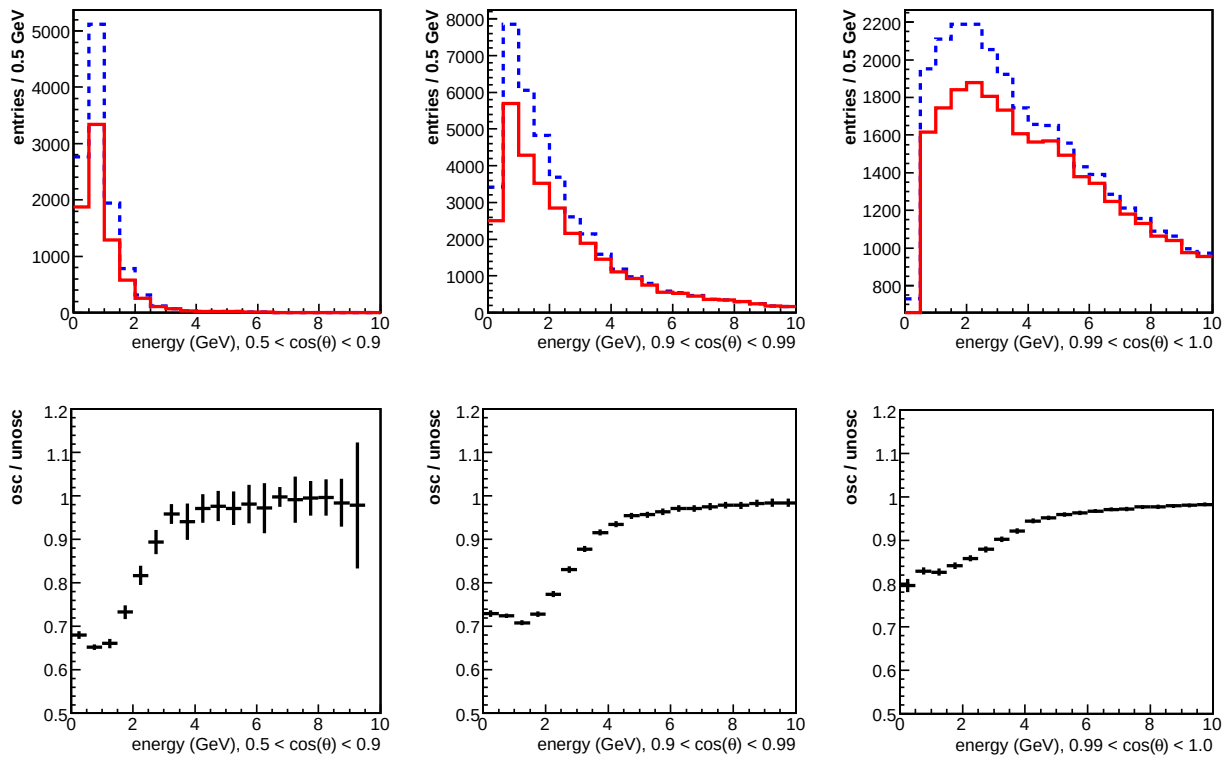

Figure 3: Track energy distributions in different angle ranges (top) and the ratios between oscillated and un-oscillated distributions (bottom).

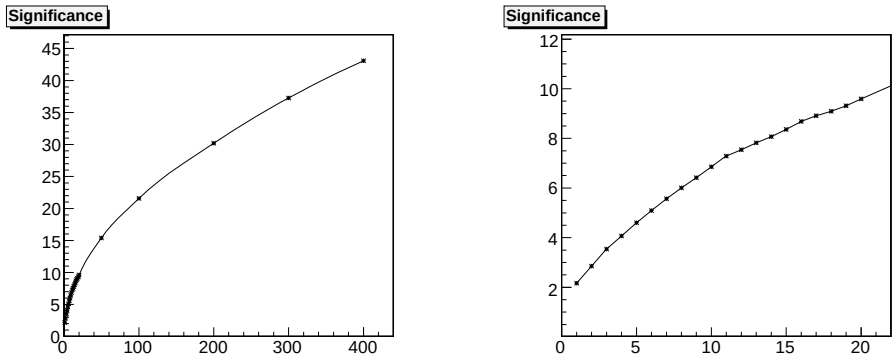

Figure 4: Significance as a function of the number of POT. The RHS plot is a zoom-in of the LHS one where the POT range is from 0 to 20×10^{20} POT.

3 Rate Only Sensitivity Estimates

We study the rock muon sensitivity to the oscillation parameters $sin^2 2\theta = 0.95$ and $\Delta m_{32} = 3.0 \times 10^{-3}\ eV^2$ as a function of the number of protons on target. First, we adopt a simple approach in which we only account for the rock muon rate difference between oscillating and non-oscillating neutrinos. Our MC sample contains a total of $N = 109272$ events corresponding to 554.67×10^{20} POT. With this, the number of events corresponding to X POT is $N_X = X \times 109272/554.67 \times 10^{20}$ POT. We select successive samples of 1, 2 up to 20 POT and then 50, 100, 200, 300 and 400 POT. For each of these samples we calculate the total number of selected events N_{un-osc} and the total number of survived events N_{surv}. We define the significance of the observed depletion in the number of rock muons as:

$$S = \frac{N_{un-osc} - N_{surv}}{\sqrt{N_{un-osc}}}. \tag{2}$$

Figure 4 shows the significance as a function of the number of POT. Currently we have about 1.4×10^{20} POT which corresponds to a significance of 2.5σ. By the end of the MINOS running we expect to accumulate about 7.0×10^{20} POT which would correspond to a $5\,\sigma$ significance of a oscillation measurement. More precisely, with rock muons, we will be able to exclude the non-oscillation hypothesis at $5\,\sigma$ level if we use a rate only analysis. It is clear, however, that a rate only analysis is not an optimal choice. Using the energy and angular distributions of the rock muons will clearly improve the sensitivity to neutrino oscillations [1]. Including the contained vertex events rejected by the main charge-current analysis will also result in significant improvement.

4 Oscillation Fit

To determine the oscillation parameters $sin^2 2\theta$ and Δm_{32} we develop a fitter that uses the maximum likelihood method. To test the fitter on the Monte Carlo sample, we use the following method. We divide the Monte Carlo sample in two equal subsamples. We treat the first subsample as "mock data". Given certain oscillation parameters we construct the

oscillated two-dimensional energy-θ_{beam} distributions as they would be observed in real data. We can construct the oscillated energy-θ_{beam} distributions to correspond to any number of POTs between 0 and $277\times10^{20} = 554/2 \times10^{20}$. From the second subsample we construct "trial" energy-θ_{beam} distributions corresponding to "trial" $sin^2 2\theta$ and Δm_{32} pairs. We use a grid scan of 50×50 in which $sin^2 2\theta$ is varied between 0 and 1.4 and Δm_{32} varies between 0 and 12.0e-3 eV^2. For each oscillation parameter pair, the "trial" energy-θ_{beam} distribution is compared with the distribution "observed" in the "mock data". The energy-θ_{beam} distributions are represented by 10 (energy) by 3 (angle) 2D histograms. The energy range is from 0 to 10 GeV and the $\cos(\theta_{beam})$ range is from 0.5 to 1. The "trial" histograms are initially constructed using all events in the second subsample ($\approx$277 $\times10^{20}$ POT). Then, they are scaled down by the ratio between the number of POT in the observed histogram and the number of POT in the trial histogram. This way, both the observed and trial histograms correspond to the same number of POT, but the trial one has suppressed statistical fluctuations. In what follows we neglect the statistical fluctuations in the trial distributions since the size of the Monte Carlo subsample ($\approx$227 $\times10^{20}$ POT) used to produce them is at least an order of magnitude larger than any data sample that can be accumulated at MINOS.

For each bin, the probability of observing N_{obs} events when N_{exp} are expected is given by the Poisson probability:

$$P(N_{obs}, N_{exp}) = e^{-N_{exp}} \frac{N_{exp}^{N_{obs}}}{N_{obs}!} \tag{3}$$

The normalized likelihood is defined as:

$$L = \prod_i \frac{P(N_{obs,i}, N_{exp,i})}{P(N_{exp,i}, N_{exp,i})} = \prod_i \frac{e^{-N_{exp,i}} N_{exp,i}^{N_{obs,i}}}{e^{-N_{obs,i}} N_{obs,i}^{N_{obs,i}}}, \tag{4}$$

where the index i runs over all energy and angle bins in the 2D histograms. The approximate χ^2 probability is defined as:

$$\chi^2 = -2 \times ln(L). \tag{5}$$

5 Tests of the Oscillation Fit

To test the fitting procedure for 2.5×10^{20} POT we set the input oscillation parameters at two different values: $\{sin^2 2\theta, \Delta m_{32}^2\} = \{(0.95, 3.0 \times 10^{-3}\ eV^2), (0.50, 5.0 \times 10^{-3}\ eV^2)\}$. For each pair, we set the numbers of energy and $\cos(\theta_{beam})$ bins in three different configurations. In the first configuration we have only one energy and one angle bin. This is equivalent to a rate-only analysis in which we simply count all rock muon events with energy between 0 and 10 Gev and $\cos(\theta_{beam})$ between 0.5 and 1. In the second configuration we have 10 energy bins and one angle bin. This is an analysis in which we account for rate and shape of the energy spectrum. Finally, in the third configuration, we have 10 energy bins and three angle bins. In this way we attempt to increase the sensitivity by accounting for rate, shape of the energy spectrum and shape of the angular distribution.

Figure 5 shows the fit results corresponding to the two pairs of input parameters and three energy-angle binning configurations. The 68, 90 and 99% confidence levels are shown as

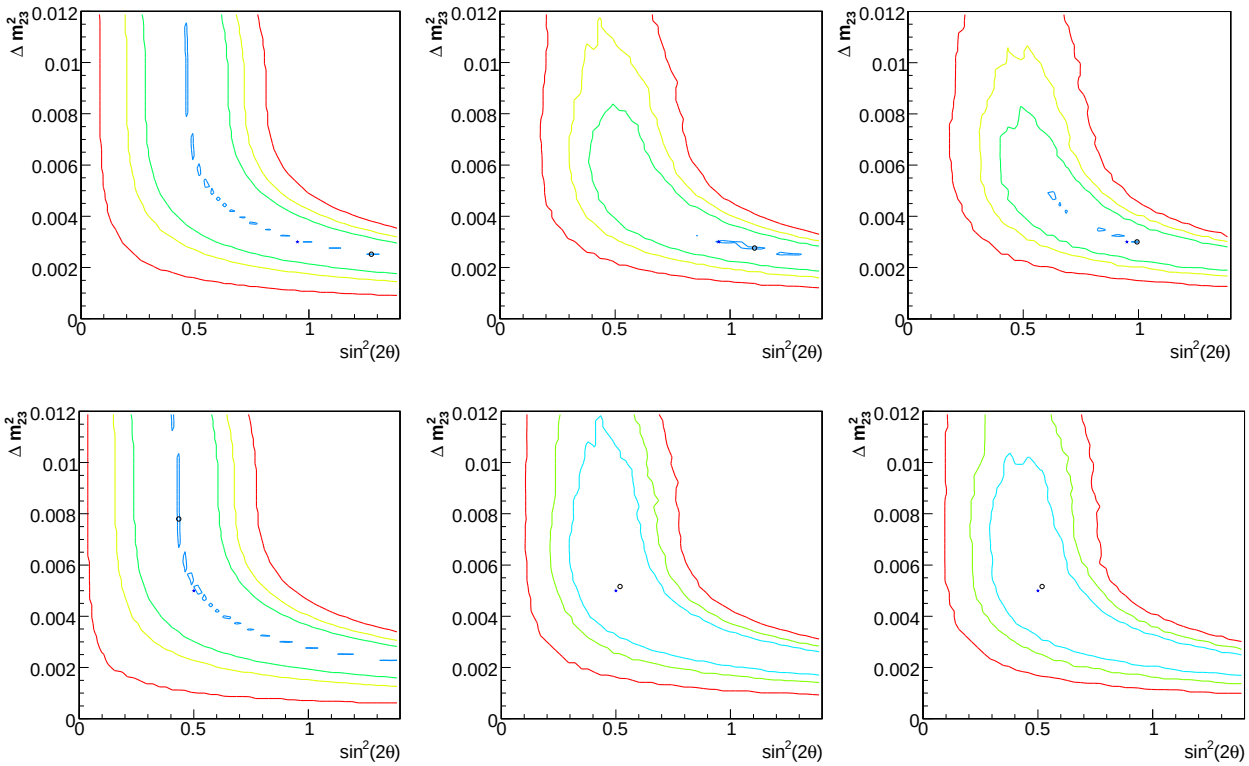

Figure 5: Fit results for $(0.95, 3.0 \times 10^{-3}\ eV^2)$ (top) and $(0.50, 5.0 \times 10^{-3}\ eV^2)$ (bottom); rate-only (left) rate+energy dependence (middle), rate+energy+angular dependence (right). The 68, 90 and 99% confidence levels are shown in blue, green and red, respectively. The input value are shown by the blue star and the fit result by the open circle. The blue contours show a small vicinity around the maximum.

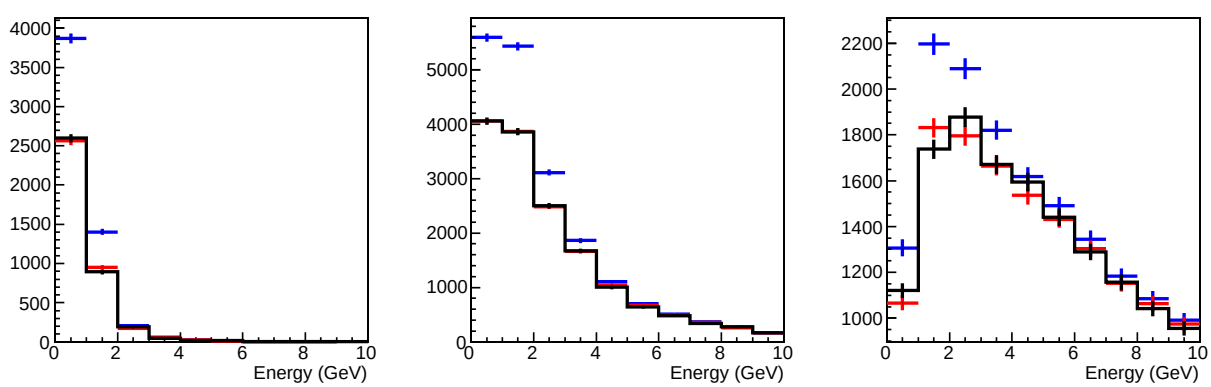

Figure 6: Energy distributions in three $\cos(\theta_{beam})$ ranges: 0.5-0.9 (top-left), 0.9-0.99 (top-right) and 0.99-1.0 (bottom-left). The unoscillated "mock data" is shown in blue. The oscillated "mock data" is shown in red. The energy distributions corresponding to the best fit are shown in black.

the section from the $\chi 2$ surface where the distance from the minimum $\Delta\chi 2$ is 2.30, 4.61 and 9.21 respectively. To suppress statistical fluctuations in the confidence contours, all "mock data" is used to generate the oscillated histogram. The histogram is then scaled down by the ratio between 2.5×10^{20} POT and the total number of POT in the "mock data" sample. In the rate-only cases, the input and fit output oscillation parameters seem to be quite far apart. However, they are well within the 68% confidence levels. Moreover, we plot (in blue in Figure 5) the contour for which $\Delta\chi 2$ is 0.01 which corresponds to the region in which the deviation from the minimum is very small. It is clear that the minimum is not well localized, but it extends along a curve passing through the center of the confidence bands. The input and fit output are always on this minimum curve. As we add the energy shape information by using 10 energy bins we find that the confidence contours become narrower and they close for high values of Δm^2. The input and fit output parameters are closer together. Finally, we add the direction information to the fit by using 10 energy bins and 3 angular bins. The corresponding confidence contours seem to be slightly improved. Figure 6 shows the comparison between the "mock data" and the best fit energy distributions corresponding to each $\cos(\theta_{beam})$ range.

In Appendix 2 we investigate the reasons for the observed deviations between the input and fit output values discussed above.

We continue by investigating the statistical fluctuations of measurements with limited size data samples. We divide the "mock data" sample in sub-samples of 1.3, 2.5, 5.0, 10.0 and 20.0×10^{20} POT corresponding to ensembles of 213, 110, 55, 27 and 13 pseudo-experiments, respectively. The number of events in the subsamples are chosen so that they are distributed according to Poisson statistics with a mean given by the total number of events in the "mock data" divided by the number of subsamples. For each sample size, each sub-sample is fit and the fit results are shown in Figure 7. The distribution of the fit results in the oscillation parameter space follows the confidence contours as expected.

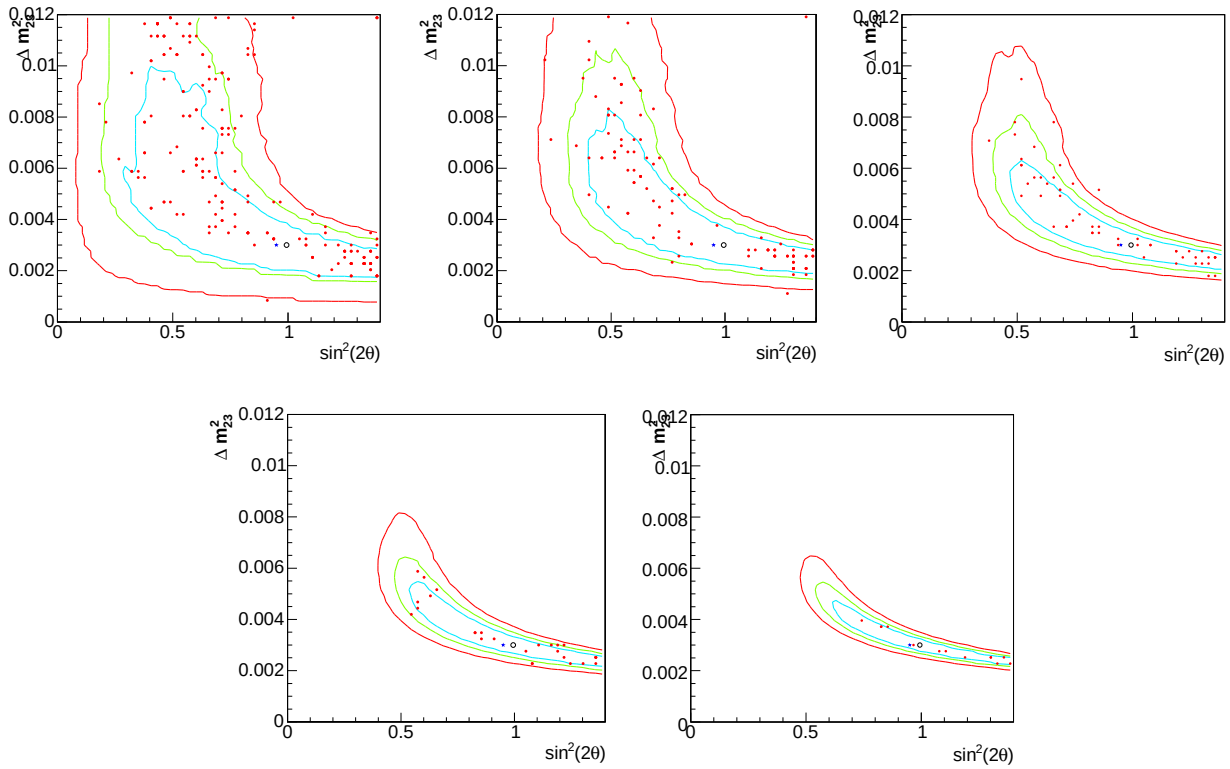

Figure 7: Ensembles of pseudo-experiments with 1.3, 2.5, 5.0, 10.0 and 20.0×10^{20} POT.

6 Contained Vertex Events

Until now, we only studied actual rock muon events. However we find that there is a substantial fraction of contained vertex events that pass the rock muon selection requirements described in Section 2. We use a Monte Carlo sample generated with gminos_batch_carrot_06 and reconstructed with R1.18.2 minossoft. The sample has 160536 events, corresponding to an exposure of 290.6×10^{20} POT. A sample of 7236 events pass the rock muon selection criteria, out of which 5147 events survive after oscillation (assuming oscillation parameters of 0.95 and 0.0030 eV^2). In a data sample with events passing the rock muon selection criteria we expect 11.7% to be contained vertex events. This fraction depends on the selection cuts and increases with relaxed cuts. Table 2 shows a summary of the number of events in both the rock muon and the contained vertex sample. Figure 8 shows the best fit projection corresponding to 227×10^{20} POT. Since the contained vertex MC sample contains only (290.6/2)×10^{20} POT, we scale up the contained vertex distributions to the same number of POT as the rock muon events. As expected, the addition of the contained vertex events in the simulated sample slightly improves the measurement of the neutrino oscillation parameters. This effect is visible in Figure 9. Clearly, in the real data both the rock muon and the contained vertex events will be present.

One way to improve this analysis is to relax the requirements for the rock muon selection. One possibility is to select all events that are rejected by the main charged-current (CC) analysis. The CC analysis requires $r^2 < 14.0\,m^2$ and $Z_{vtx} > 0.5\,m$. With good approximation

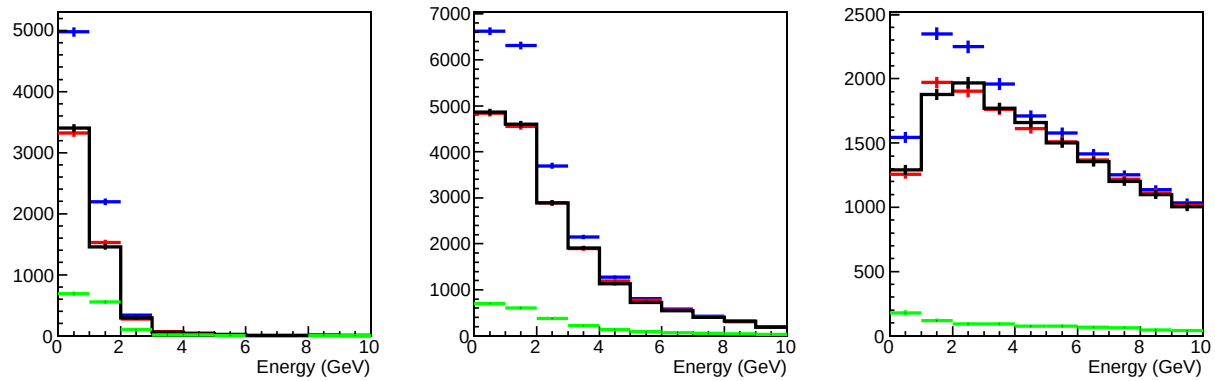

Figure 8: Energy distributions in three $\cos(\theta_{beam})$ bins for both rock muons and contained vertex events without (blue) and with (red) oscillations. The oscillated contained vertex component is also shown (green). The best fit projection is superimposed (black).

	Rock Events	Contained Vertex Events
POT ($\times 10^{20}$)	554.67	290.60
Total	109272	160536
Selected	97872	7263
Survived	83425	5147
POT ($\times 10^{20}$)	1.3	1.3
Total	256.1	718.2
Selected	229.4	32.5
Survived	195.5	23.0

Table 2: Number of events in the rock muon sample and in the contained vertex sample. The total number of events as well as the number of events that pass the rock muon selection cuts (described in Section 2) and the number of muons that survive after oscillations are shown. The numbers of events scaled down to correspond to 1.3×10^{20} POT are also shown.

we select the events rejected by these cuts by requiring that the distance from the detector surface be less that 0.5 m and that the track vertex is no more than 9 planes from the detector faces. In a next iteration of this analysis we will use the exact inverse CC cuts.

As seen in Table 3, releasing the cuts, slightly increases the number of rock muons but increases the number of contained vertex events by a factor of 5. The table also shows the numbers of muon tracks that enter the front face of the detector and the number of tracks that enter the lateral surface. The confidence contours corresponding to each subsample are shown in the Apendix. Since in this analysis we only use the muon information, we need not worry about partially reconstructed showers of contained events that occur at the edges of the detector. The improvement of the confidence contours when using the inverse CC cuts is clearly seen in Figure 9 while the fit projection is shown in Figure 10 .

We study the integrity of the fit procedure, as before, by using a high statistics MC sample. The input and the fit results are shown in Figure 11. The distribution of pseudo-

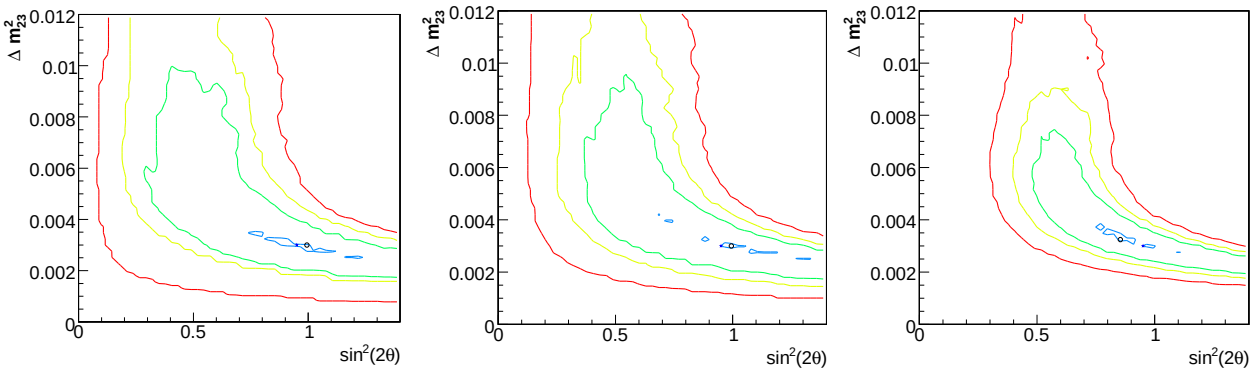

Figure 9: Confidence contours (68% - green, 90% - yellow, 99% - red, small vicinity arround the minimum obtained by varying the χ^2 by 0.1 - blue) for a 1.3×10^{20} POT sample corresponding to rock muons only (left), rock muons and contained vertex events with initial selection requirements (middle) and rock muons together with contained vertex events with inverse CC selection cuts.

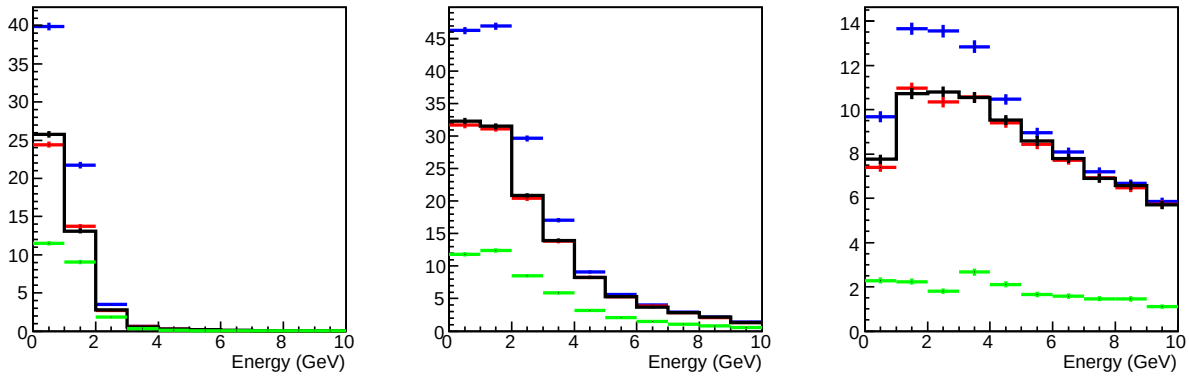

Figure 10: Energy distributions with inverse CC cuts in three $\cos(\theta_{beam})$ ranges: 0.5-0.9 (top-left), 0.9-0.99 (top-right) and 0.99-1.0 (bottom-left). The unoscillated "mock data" is shown in blue. The oscillated "mock data" is shown in red. The oscillated contained vertex component is also shown (green). The best fit projection is superimposed (black).

experiments for 1.3, 2.5 and 5.0×10^{20} POT are shown as well. The confidence contours for these sample sizes are obtained by scaling down the muon distributions accordingly. As a result, these contours are free of statistical fluctuations. To see the contour shapes for an actual sample of 1.3×10^{20} POT, we select three independent samples, each containing 1.3×10^{20} POT. The confidence contours and the best fit projections are shown in Figure 12. These are the contours and muon energy distributions that we expect to see in the present data sample corresponding to 1.3×10^{20} POT.

	Rock Events	Contained Vertex Events
POT ($\times 10^{20}$)	554.67	290.60
Total	109272	160536
Selected	100403	33770
Survived	85625	23018
- front face	51046	2149
- lateral surface	34579	20869
POT ($\times 10^{20}$)	1.3	1.3
Total	256.1	718.2
Selected	235.3	151.1
Survived	200.7	103.0
- front face	119.6	9.6
- lateral surface	81.1	93.3

Table 3: Number of events in the rock muon sample and in the contained vertex sample. The total number of events as well as the number of events that pass the inverse CC selection cuts and the number of muons that survive after oscillations are shown. The numbers of events scaled down to correspond to 1.3×10^{20} POT are also shown. The numbers of survived events are divided between tracks that enter the front face of the detector and tracks that enter the lateral surface.

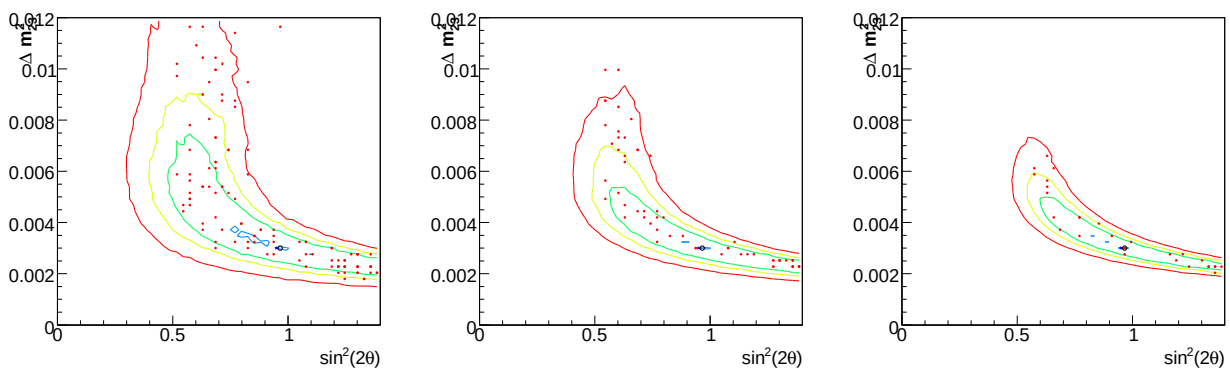

Figure 11: Ensembles of 1.3, 2.5 and 5.0×10^{20} POT. The samples contain both rock muons and contained vertex events selected with inverse CC cuts.

7 Conclusions

In this note we studied the sensitivity of rock muons to the atmospheric neutrino oscillation parameters. The initial study used rate only information. We then described the rock muon variables sensitive to neutrino oscillations, and used them to improve the sensitivity of the analysis. Finally, we tested in detail the fitting procedure and showed that we have a unbiased analysis technique.

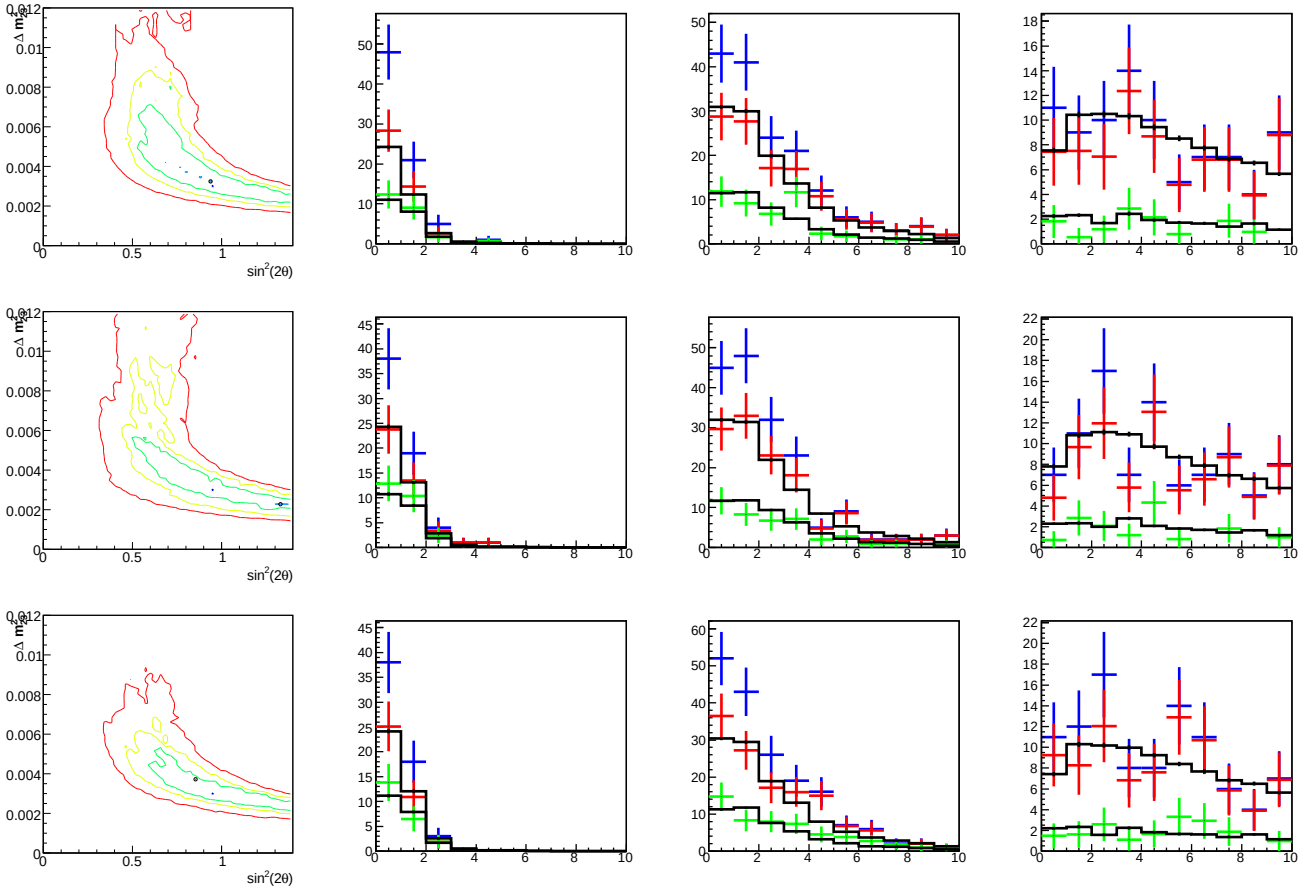

Figure 12: Three different examples of confidence contours and best fit projections for samples of 1.3×10^{20} POT each. The samples contain both rock muons and contained vertex events selected with inverse CC cuts.

8 Appendces

8.1 Appendix 1

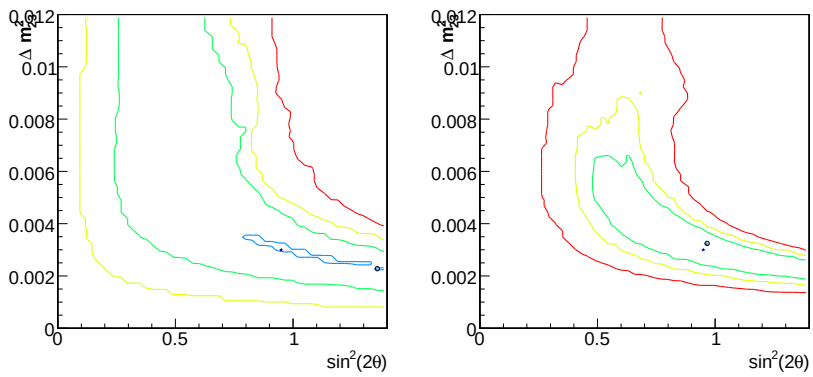

Figure 13: Confidence contours corresponding to 1.3×10^{20} POT with inverse CC cuts. Cotribution of muon tracks that enter the front face (left) and lateral surface (right).

8.2 Appendix 2

In the case of the rate-only analysis, it is clear that the fit can only resolve the values of the oscillation parameters up to a degenerate curve. However, when the energy is added we expect that the maximum be better localized. Our hypothesis is that the deviations between the input and the fit output, in the case of rate+energy and rate+energy+angle, are simple statistical fluctuations. To prove this, instead of using statistically independent subsamples for "mock data" and Monte Carlo, we use the same Monte Carlo dataset to generate both the "mock data" oscillated histograms and the trial ones. The fit results for this case are shown in Figure 14. Except for the rate-only case in which the $\chi2$ minimum is degenerate, the input and fit output parameters are almost identical. Figure 15 shows the comparison between the "mock data" and the best fit energy distributions corresponding to each $\cos(\theta_{beam})$ range. As expected, the best fit distributions and the mock data distributions are identical because the same sample is used.

9 Acknowledgments

We thank Juergen Reichenbacher and Tom Fields for useful discussions.

References

[1] A. McGowan, G. Giurgiu "Oscillation analysis sensitivity of rock muons in the MINOS far detector", NUMI Note 2184.

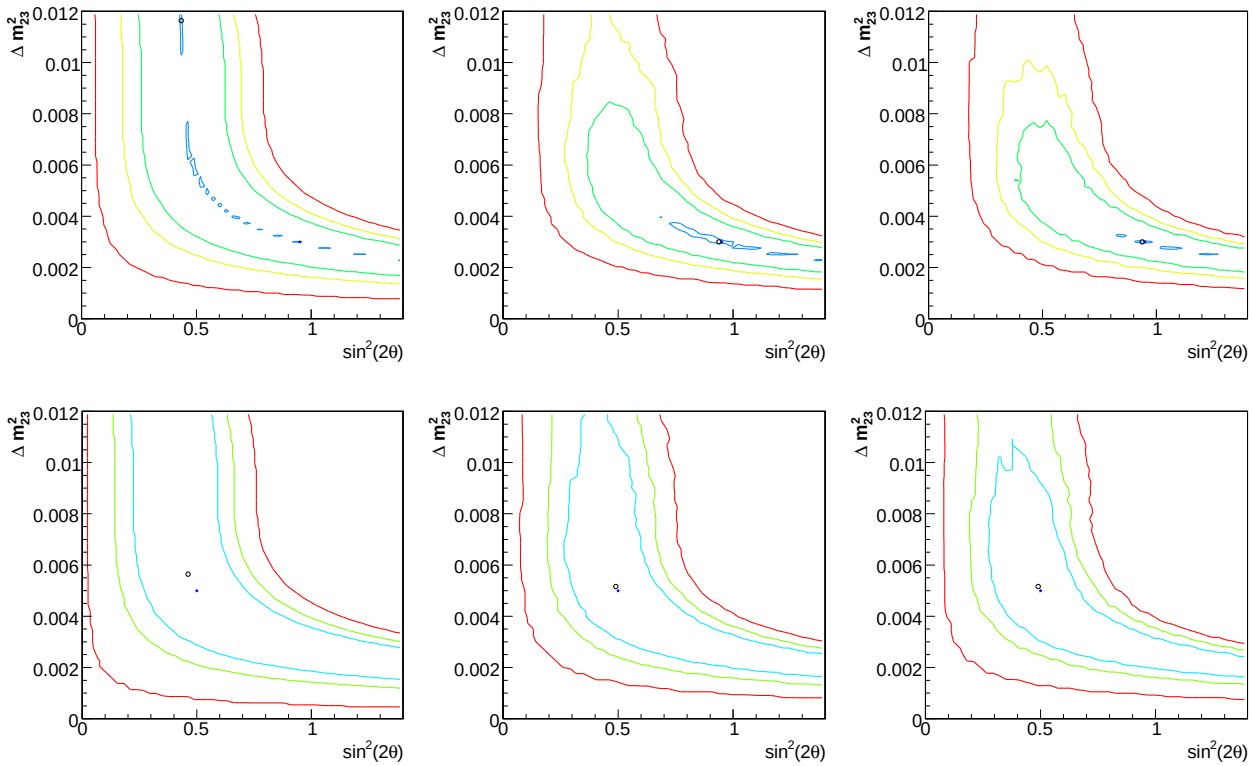

Figure 14: Statistically correlated samples: Fit results for $(0.95, 3.0 \times 10^{-3}\ eV^2)$ (top) and $(0.50, 5.0 \times 10^{-3}\ eV^2)$ (bottom); rate-only (left) rate+energy dependence (middle), rate+energy+angular dependence (right). The 68, 90 and 99% confidence levels are shown in blue, green and red, respectively. The input value are shown by the blue star and the fit result by the open circle.

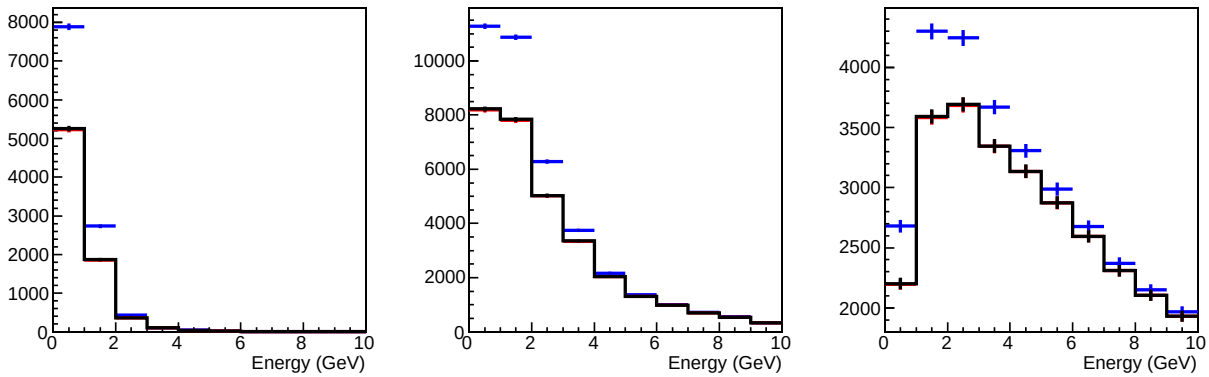

Figure 15: Energy distributions in three $\cos(\theta_{beam})$ ranges: 0.5-0.9 (top-left), 0.9-0.99 (top-right) and 0.99-1.0 (bottom-left). The unoscillated "mock data" is shown in blue. The oscillated "mock data" is shown in red. The energy distributions corresponding to the best fit are shown in black.